United block sequence mapping-based visible light positioning for dense small cell deployment

Runmei Zhao (赵润美), Zhitong Huang (黄治同), Yuxin Liu (刘雨欣), and Yuefeng Ji (纪越峰)*

State Key Laboratory of Information Photonics and Optical Communications, Beijing University of Posts and Telecommunications, Beijing 100876, China

**Corresponding author: jyf@bupt.edu.cn*

Received December 15, 2015; accepted April 22, 2016; posted online June 9, 2016

Visible light positioning (VLP) is an emerging candidate for indoor positioning, which can simultaneously meet the requirements for accuracy, cost, coverage area, and security. However, intercell interference caused by light intensity superposition limits the application of VLP. In this Letter, we propose a united block sequence mapping (UBSM)-based VLP that utilizes superposition to integrate the multidimensional information from dense small cells into 2D information. The experimental result shows that UBSM-based VLP can achieve an accuracy of 1.5 cm with a 0.4 m row spacing and 0.35 m column spacing of LED lights.

OCIS codes: 060.4510, 200.2605, 230.3670.

doi: 10.3788/COL201614.070601.

Indoor positioning is playing an important role in security monitoring, object tracking, and indoor navigation. There are many indoor positioning technologies, such as ultra-wide band (UWB), radio frequency identification (RFID), wireless local area network (WLAN), and Bluetooth[1]. However, they all have limitations. RF-based positioning technologies are not secure as the RF signals can penetrate walls. The high cost of UWB equipment makes it unsuitable for broader use. The spectrum that Bluetooth uses is unlicensed and is vulnerable to interference from a wide range of signal types using the same frequency.

An unprecedented opportunity for visible light communication and visible light positioning (VLP) is brought by the introduction of white LEDs for illumination and extensive research has been done[2–16]. Techniques based on different parameters are applied in VLP. The angle of arrival (AOA) is used in Ref. [7], and the simulation results show that the average localization accuracy is on the order of 0.2 meters. In Ref. [8], an VLP system based on time differences of arrival (TDOA) can achieve an estimation accuracy of 3.6 cm on average in the simulation and the impact of multipath effects on the theoretical accuracy of time of arrival based indoor VLP positioning system is analyzed in Ref. [9]. In Ref. [10], the combination of visible light and an accelerometer achieves an average position error of less than 0.25 m. However, the methods mentioned above are sensitive to the light intensity superposition that appears in uniform illumination so user access[11,12] and scheduling[13] may need to be considered. In order to solve this problem, the multiple-input multiple-output[14] dual-tone multifrequency technique[15] and carrier allocation[16] are used, which achieve the average estimated position error of 1, 1.6, and 7 cm, respectively, in the experiment, but limitations still exist for dense small cell deployment that may appear in large public facilities like airports.

United block sequence mapping (UBSM)-based VLP is proposed in this Letter for dense small cell deployment. Considering that specific positioning messages can be sent suitably combined with the layout of the LED lights, UBSM-based VLP integrates the multidimensional information from dense small cells into 2D information corresponding to the position on the detection surface, namely, dimension reduction. Three positioning determination mechanisms, mapping table mechanism (MTM), mapping function mechanism (MFM), and approximate calculation mechanism (ACM) are proposed to get the position from the measured values.

In this Letter, the effect of white Gaussian noise can be eliminated by multiple sampling as its mean value is zero[17]. The diffuse channel gain can be measured previously for a given room and the proposed positioning scheme does not require a high modulation speed, so the effect caused by the multipath link can be omitted, according to Ref. [17].

The proposed positioning scheme can work when the layout of LED lights is hexagonal or rectangular. Only rectangular layout is discussed in this Letter due to the page limit. A hall (Lm $\times$ Wm $\times$ Hm) is assumed for the later analysis. The LED lights are installed at the height of Hm horizontally. Each LED light can consist of several LED chips. The receiver is laid at the height of hm horizontally. There are $M \times N$ LED lights (M rows and N columns). $\mathrm{LED}_{i,j}$ represents the LED light in the ith row and the jth column with the coordinate (x_j, y_i, H). The receiver position is (x, y, h). In this Letter, H and h that should be measured in advance so, (x_j, y_i, H) is shortened to (x_j, y_i) and (x, y, h) is shortened to (x, y).

The x–y plane is divided into small grids (M rows and N columns), according to the layout of the LED lights. The positioning frame format is used to construct the mapping relationship. We design the frame format as concise as

possible, which will help make the frame more suitable to work with other functions and simplify the frame processing design of the receiver. Bit stuffing is used to guarantee that the synchronization head can be detected correctly. 2-pulse position modulation can be used to avoid nonuniform illuminance distribution. All the LED lights transmit the positioning frame simultaneously.

The positioning frame consists of the following five parts: the synchronization head, the total number of rows (M), the total number of columns (N), the row index (RI), and the column index (CI). Before bit stuffing, the bit numbers of the five parts are 8, 8, 8, M, and N, respectively. The most effective parts of the frame format are RI and CI. They are closely linked with the position of the LED lights. RI and CI are set to have a variable length in order to adapt to the different LED light layout for different rooms. In order to decipher these two parts correctly, the other three parts are needed. The function of the synchronization head is to help the terminal recognize the beginning of the positioning frame. We use the typical '01111110' as the synchronization head. For the second third parts of the frame, M and N are expressed in binary. The maximum value of M and N are both (2^8-1), which is enough even in a large public facilities. Their function is to help terminals determine the boundary of RI and CI. RI and CI both have 2 framing modes as Table 1 illustrates. Each bit costs one bit time slot to transmit.

There are six adjacent '1' bits in the synchronization head and bit stuffing is used to ensure that this pattern can never occur in the other parts of the positioning frame. In this Letter, the bit stuffing rule is made below. For the second and third parts, '0' is inserted after the 4th and the 8th bit and the bit number is extended to 10. For RI, take every 5 bits as a section. If M is not divisible by 5, the bit number of the last section is less than 5. Insert a bit '0' after each section. The rule for CI is similar. Figure 1 illustrates the general design of the positioning frame format before and after bit stuffing.

Figure 2 illustrates the positioning frame of $\mathrm{LED}_{2,7}$ (M=11, N=7) before and after bit stuffing. The bits in red are inserted for bit stuffing.

Table 1. Frame Modes.

	RI of ith Row	
RI frame mode	'1' position	'0' position
'R+'	last i	first $(M-i)$
'R−'	last $(\mathrm{M}+1-i)$	first $(M-i)$
	CI of j column	
CI frame mode	'1' position	'0' position
'C+'	last (j)	first $(N-j)$
'C−'	last $(\mathrm{N}+1-j)$	first $(j-1)$

'R+''C+' frame is used in the remainder of the Letter.

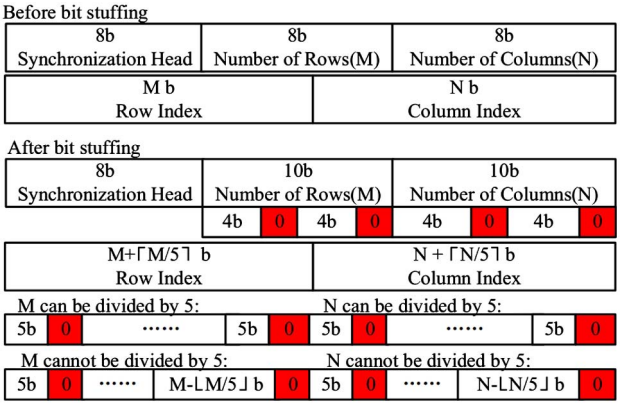

Fig. 1. General design of the positioning frame.

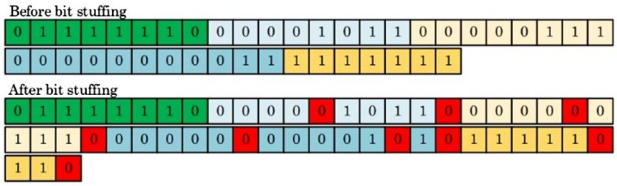

Fig. 2. Positioning frame of $\mathrm{LED}_{2,7}$ ($M=11$, $N=7$).

The received signal strength (RSS) of each bit time slot of RI or CI needs to be summed and then divided by the RSS of the last bit time slot of RI or CI. $\mathrm{RSS}_{i,j}$ represents the RSS of $\mathrm{LED}_{i,j}$ and the relevant analysis can be found in Ref. [18]. The processing of RI or CI for point (x, y) can be expressed concisely in matrix form:

$$\alpha_R(x,y) = (W_R * S_R)/(O_R * S_R), \tag{1}$$

$$W_R = \begin{bmatrix} 1 & 2 & \dots & M \end{bmatrix}, \tag{2}$$

$$S_R = [\, S_{\mathrm{Row}\,1}(x,y) \quad S_{\mathrm{Row}\,2}(x,y) \quad \dots \quad S_{\mathrm{Row}\,M}(x,y)\,]^{\,T}, \tag{3}$$

$$O_R = \begin{bmatrix} 1 & 1 & \dots & 1 \end{bmatrix}, \tag{4}$$

$$S_{\mathrm{Row}\,i}(x,y) = \sum_{j=1}^{N} \mathrm{RSS}_{i,j}, \tag{5}$$

where $\alpha_R(x, y)$ is the row mapping result at point (x, y), S_R is an $M \times 1$ matrix and its element, $S_{\mathrm{Row}\,i}(x, y)$ represents the RSS from the LED lights in the ith row, the ith element of W_R is equal to the number of bit '1' in RI for the LED lights in the ith row and in this Letter it is a vector with elements of 1 to M, and O_R is an all-1 vector with a size of $1 \times M$.

$$\alpha_C(x,y) = (W_C * S_C)/(O_C * S_C), \tag{6}$$

$$W_C = \begin{bmatrix} 1 & 2 & \dots & N \end{bmatrix}, \tag{7}$$

$$S_C = [\, S_{\mathrm{Col}\,1}(x,y) \quad S_{\mathrm{Col}\,2}(x,y) \quad \dots \quad S_{\mathrm{Col}\,N}(x,y)\,]^{\,T} \tag{8}$$

$$O_C = \begin{bmatrix} 1 & 1 & \dots & 1 \end{bmatrix}, \tag{9}$$

$$S_{\mathrm{Col}\,j}(x, y) = \sum_{i=1}^{M} \mathrm{RSS}_{i,j}, \tag{10}$$

where $\alpha_C(x, y)$, S_C, $S_{\mathrm{Col}\,i}(x, y)$, W_C and O_C are similarly defined as $\alpha_R(x, y)$, S_R, $S_{Row\,i}(x, y)$, W_R, and O_R.

Solving (x, y) from $\alpha_R(x, y)$ and $\alpha_C(x, y)$ is difficult. Hence, we propose three mechanisms, MTM, MFM and ACM, to solve this problem. Notably, $\alpha_R(x, y)$ for a certain x and $\alpha_C(x, y)$ for a certain y in the positioning area has to be monotonical to guarantee one-to-one correspondence.

The fingerprint database mechanism (FDM)[19] and three proposed mechanisms are explained here. α_{Rm} and α_{Cm} are the row and column mapping results for a certain point calculated by the measured RSS. Suppose that there are mm row sample nodes and nn column sample nodes.

The fingerprint database contains $(mm \times nn \times M \times N)$ RSS as the RSS of each LED light for each sample node needs to be recorded. Choose the position of the sample node that has the minimum mean square error (MSE) between the measured RSS and the corresponding offline $M \times N$ RSS as the receiver position.

The first step of MTM is to establish the database. There should be $(mm \times nn)$ values calculated by $\alpha_R(x, y)$ and $(mm \times nn)$ values calculated by $\alpha_C(x, y)$, which constitutes α_R matrix $(mm \times nn)$ and α_C matrix $(mm \times nn)$. The mm ordinate values and the corresponding row mapping results are stored in row mapping table (r-MT) and the corresponding row mapping results $(mm \times 1)$ are row average values of α_R matrix $(mm \times nn)$. The column mapping table (c-MT) can be obtained in a similar way. After this step, the scale of the database can decrease to $(mm + nn)$, which leads to a faster positioning. Notably, the generation step limits the accuracy because the elements of α_R matrix in a row or α_C matrix in a column are similar but not the same and the smaller $(\partial\alpha_R(x, y))/\partial$x and $(\partial\alpha_C(x, y))/\partial$y are, the more accurate the positioning results can be obtained. Finally, the receiver position (x, y) is determined by r-MT and c-MT.

The performance of MTM is dependent on the scale of the database; in other words, the spacing of the sample nodes. The larger the database is, the better the accuracy performance is, but the time it costs is longer and the storage it needs is larger. Therefore, MFM is proposed. Row mapping function (r-MF) and column mapping function (c-MF) can be generated by MTs. The dependent variable is abscissa x or ordinate y and the independent variable is α_R or α_C. The MFs can be fitted into certain polynomial functions. In order to equilibrate the system complexity and the positioning accuracy, the degree of polynomial functions should increase until the MSE between MTs and the corresponding values calculated by MFs decreases to the acceptable level. In the remainder of this Letter, MF(k) represents the degree of MF k and MFM(k) represents MFM using MF(k). Notably, MFM$(2k-1)$ and MFM$(2k)$, $(k \geq 1)$ are nearly the same for symmetrical layouts. Finally, x is calculated by substituting α_{Cm} into (c-MF) and y is calculated by substituting α_{Rm} into (r-MF).

Both MTM and MFM need offline training, which is hard to implement when the positioning area is large, so ACM is proposed. Figure 3 illustrates its procedures. The receiver position (x, y) should be calculated from $\alpha_R(x, y) = \alpha_{Rm}$ and $\alpha_C(x, y) = \alpha_{Cm}$, which is a difficulty. In order to solve this problem, both the Newton–Raphson method and binary search method are used in ACM.

In ACM, x and y are obtained one by one from $f_C(x) = 0$ and $f_R(y) = 0$, where $f_C(x)$ and $f_R(y)$ are defined as

$$f_R(y) = \alpha_R(x_s, y) - \alpha_{Rm}, \tag{11}$$

$$f_C(x) = \alpha_C(x, y_s) - \alpha_{Cm}, \tag{12}$$

where x_s and y_s are the selected values to ensure x and y can be solved separately. x_0, the initial value of x_s, is calculated by Eq. (13) in 'C+' frame or Eq. (14) in 'C−' frame. y_0, the initial value of y_s, is calculated by Eq. (15) in 'R+' frame or Eq. (16) in 'R−' frame.

$$x_0 = \min(x) + \frac{(\max(x) - \min(x))}{(N-1)} * (\alpha_{C_m} - 1), \tag{13}$$

$$x_0 = \max(x) - \frac{(\max(x) - \min(x))}{(N-1)} * (\alpha_{C_m} - 1), \tag{14}$$

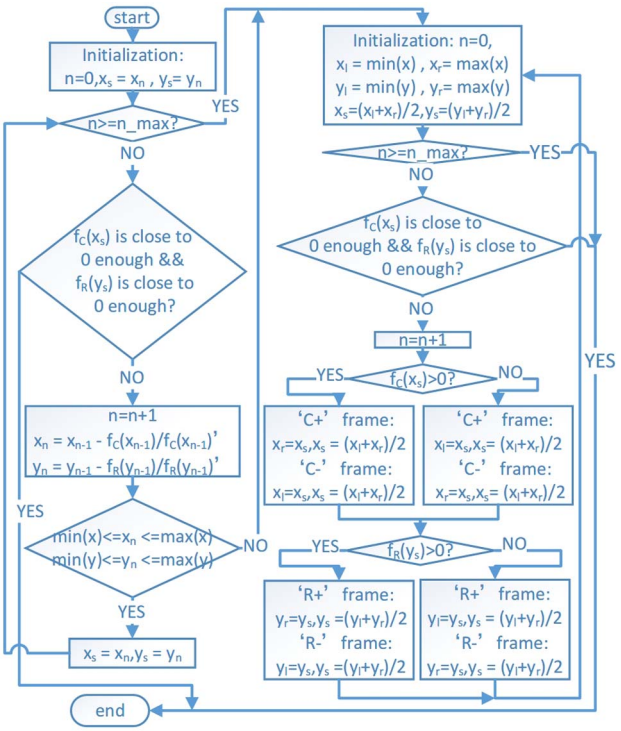

Fig. 3. Procedures of ACM.

$$y_0 = \min(y) + \frac{(\max(y) - \min(y))}{(M-1)} * (\alpha_{R_m} - 1)\ , \quad (15)$$

$$y_0 = \max(y) - \frac{(\max(y) - \min(y))}{(M-1)} * (\alpha_{R_m} - 1), \quad (16)$$

Each pair of iterations in the Newton–Raphson method is implemented as

$$x_n = x_{n-1} - \frac{f_C(x_{n-1})}{f_C(x_{n-1})'}, \qquad n \geq 1, \quad (17)$$

$$y_n = y_{n-1} - \frac{f_R(y_{n-1})}{f_R(y_{n-1})'}, \qquad n \geq 1. \quad (18)$$

x_s and y_s are updated by x_n and y_n. These steps repeat until $f_C(x_s)$ and $f_R(y_s)$ are close enough to 0 or $n \geq n\_\max$, where n is the number of iterations and $n\_\max$ is the maximum number of iterations.

In the iteration, boundary detection is needed to avoid converging to another root outside the positioning area.

Once x_n or y_n is out of the positioning area or $n \geq n\_\max$, a binary search is used to find the position. In the binary search, the range of x is $x_l \leq x \leq x_r$ and the range of y is $y_l \leq y \leq y_r$. x_l is initialed as $\min(x)$, x_r is initialed as $\max(x)$, and x_s is always $(x_l + x_r)/2$. y_l is initialed as $\min(y)$, y_r is initialed as $\max(y)$, and y_s is always $(y_l + y_r)/2$. In every iteration, either x_l or x_r is updated by x_s and either y_l or y_r is updated by y_s. The stop condition for the binary search is the same as for the Newton–Raphson method (x_s, y_s), which is the positioning result.

In the simulation, the room size is 20 m × 20 m × 6 m to simulate a large indoor venue where dense small cells are more likely to occur. The LED lights are installed at the height of 6 m. The height of the receiver is 0.85 m. There are 10 × 10 LED lights. In order to quantitatively describe the superposition for dense small cell deployment, the degree of superposition (DOS) is defined as the number of LED lights whose light can be detected at that point. Figure 4(a) shows the distribution of the normalized received optical power and the layout of the LED lights. Figure 4(b) shows the DOS on the detection surface. As seen in Fig. 4, the illumination is uniform in most parts of the room and the DOS can even reach 65, which makes many existing VLP methods unsuitable to use. The details of the parameters in the simulation are summarized in Table 2.

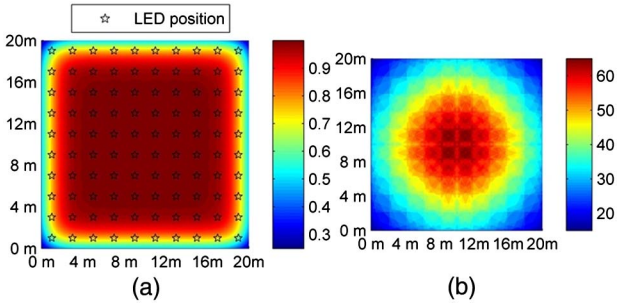

Fig. 4. (a) Distribution of the normalized received optical power and the layout of the LED lights. (b) The DOS on the detection surface.

Table 2. Simulation Parameters

Semi-angle at half power (deg.)	20
column spacing of LED lights (m)	2
Row spacing of LED lights (m)	2
Number of LED lights	100 (10 × 10)
LED installation height (ceiling height) (m)	6
FOV at a receiver (deg.)	60
Detector physical area of a PD (cm^2)	1.0
Gain of an optical filter	1.0
Refractive index of a lens at a PD	1.5
O/E conversion efficiency (A/W)	0.53

For ease of comprehension, data processing of RI is illustrated in Fig. 5. The RSS of each bit time slot of RI needs to be summed and then divided by the RSS of the last bit time slot of RI.

In the simulation, the performances on accuracy, time cost, and storage cost are compared among FDM, MTM, MFM(1), MFM(3), MFM(5), MFM(7), MFM(9), and ACM. The performance accuracy is evaluated by the mean distance error (MDE). The storage cost is evaluated by the scale of the database. The spacing of sample nodes is 0.5 m. 100 detection nodes are randomly generated on the detection surface. Table 3 shows the simulation results.

ACM achieves the best accuracy performance of these mechanisms and its positioning accuracy reaches 10^{-5} m

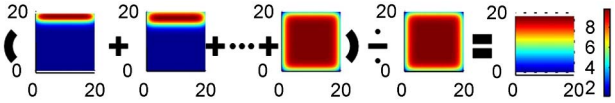

Fig. 5. Data processing of RI.

Table 3. Performance Comparison

	MDE (cm)	Time cost(s)	Storage cost
FDM	18.213	1.1074×10^{-2}	$41 \times 41 \times 100$
MTM	18.298	6.8763×10^{-5}	$41 + 41$
MFM(1)	33.2165	2.1564×10^{-4}	2×2
MFM(3)	18.918	1.5798×10^{-4}	4×2
MFM(5)	9.8284	1.4348×10^{-4}	6×2
MFM(7)	4.7849	1.4898×10^{-4}	8×2
MFM(9)	3.0163	1.4710×10^{-4}	10×2
ACM	8.33×10^{-3}	1.4526×10^{-3}	0

level. FDM and MTM achieve the same accuracy level of 0.2 m. For MFM of different degree, the larger the degree is, the better the accuracy performance can be obtained and MFM(9) can reach 10^{-2} m level. Although FDM and MTM achieve the same accuracy level, FDM costs the most time and MTM costs the least time. The time cost by MFM is in the order of 10^{-4} s and ACM costs a little longer time of 10^{-3} s. The storage cost of ACM is zero because it does not need a database. The storage cost of MFM is dependent on the degree and is not much. The storage cost of MTM and FDM are both relevant to the number of row sample nodes and column sample nodes. However, FDM always costs the most storage, which is $(mm * nn * M * N)$, while the storage costs by MTM is only $(mm + nn)$.

Note that the above discussion is on the condition that the spacing of sample nodes is 0.5 m for FDM, MTM, and MFM. If the spacing of sample nodes decreases the accuracy performance will be better. However, the more the sample spacing decreases, the harder the offline training becomes. The proposed positioning scheme is designed for the 2D scenario. In addition, only 3–5 cm error increase may occur if the difference between the actual height and the assumed height is 20 cm, according to the simulation, which is still acceptable for indoor positioning.

A concise experiment is implemented to prove the feasibility. The layout of the LED lights is 2×2 and $H - h = 0.55$. The row and column spacing of the LEDs are 0.4 and 0.35 m, respectively. Four LED lights are installed at (0.10,0.09), (0.10,0.49), (0.45,0.09), and (0.45,0.49), respectively. The spacing of sample nodes is 10 cm and the spacing of detection nodes is 5 cm. Each LED light consists of 7 LED chips (LUW JNSH.PC-CPCR-5C8 E-1). A commercially available APD (Hamamastu C12702-12) is used to detect the optical signal. The effective area of the APD is 7.0 mm^2. Figure 6 shows the experimental setup.

Figure 7 and Table 4 show the experiment result, which is nearly in accord with the simulation result. In Fig. 7, the pentacles represent the actual positions and the circles represent the estimated positions.

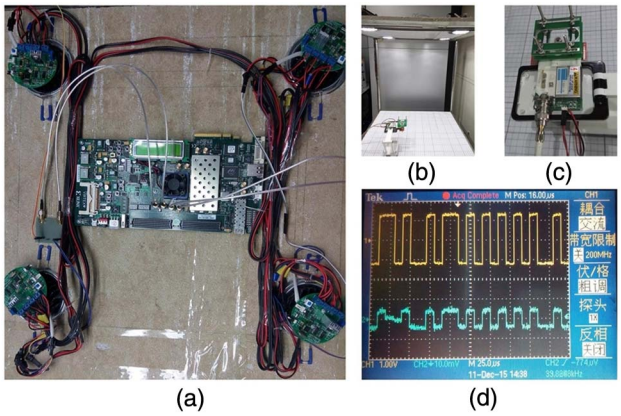

Fig. 6. (a) Control circuit of LED lights, (b) the full view of the experimental setup, (c) the APD (d) the signal of one LED light (yellow), and the received signal (blue).

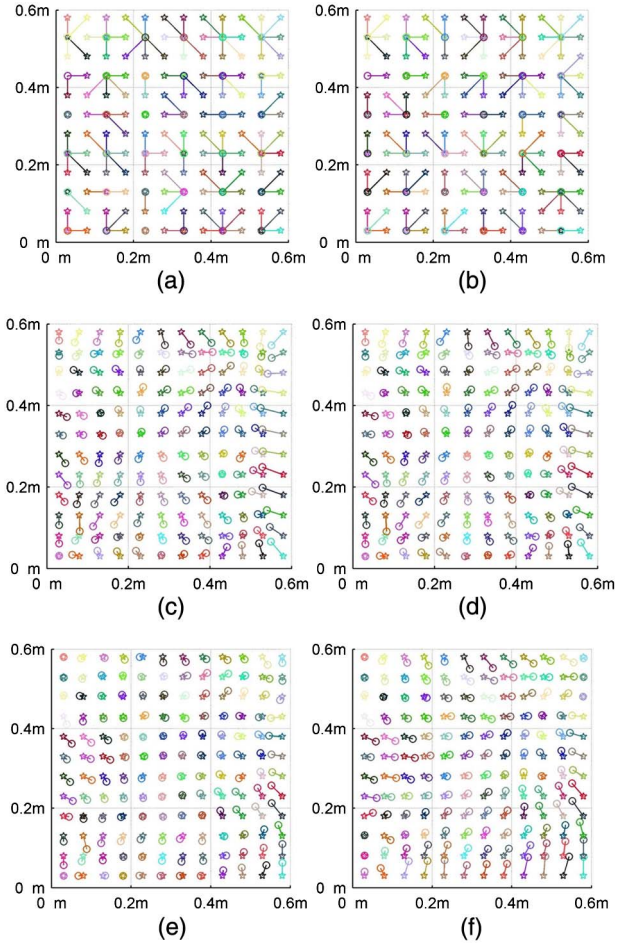

Fig. 7. Position results of (a) FDM, (b) MTF, (c) MFM(1), (d) MFM(2), (e) MFM(3), and (f) ACM.

As seen in Fig. 7 and Table 4, FMD and MTM perform the worst in the aspect of accuracy as the spacing of sample nodes is not small enough. However, the time cost by FDM and MTM are less than the other mechanisms because the experimental positioning area is small, which also makes the storage cost by FDM acceptable. MFM(3) gets a rather accurate positioning result with the MDE of 1.1929 cm, which is better than MFM(1) and MFM(2). The MDE of ACM is 1.4598 cm and the main reason is that ACM is more sensitive to parameter error.

Table 4. Performance Comparison in the Experiment

	MDE (cm)	Time cost (s)	Storage cost
FDM	4.2678	1.8635×10^{-5}	$6 \times 6 \times 4$
MTM	4.2678	1.1162×10^{-5}	$6+6$
MFM(1)	2.0060	4.8981×10^{-5}	$2+2$
MFM(2)	1.9300	3.7259×10^{-5}	$3+3$
MFM(3)	1.1929	3.9496×10^{-5}	$4+4$
ACM	1.4598	1.1×10^{-3}	0

In conclusion, UBSM-based VLP is feasible for dense small cell deployment. Moreover, the three proposed positioning determination mechanisms should be adopted according to the size of the positioning area. ACM is more suitable for large area positioning as it does not require offline training to get the database, whereas MTM and MFM are more suitable for small area positioning as they are more robust for parameter error.

This work was supported in part by the National 973 Program of China (No. 2013CB329205) and the National Science Foundation of China (No. 61401032).

References

1. M. A. Al-Ammar, S. Alhadhrmi, A. Al-Salman, A. Alarifi, H. S. Al-Khalifa, A. Alnafessah, and M. Alsaleh, in *Proceedings of International Conference on Cyberworlds* (2014), p. 245.
2. L. Kong, H. Shen, W. Xu, H. Zhang, C. Zhao, and X. You, Sci. China Inf. Sci. **58**, 82310 (2015).
3. X. Liu, A. Yang, Y. Wang, and L. Feng, Chin. Opt. Lett. **13**, 120601 (2015).
4. J. Quan, B. Bai, S. Jin, and Y. Zhang, Chin. Opt. Lett. **12**, 052201 (2014).
5. J. Tan, Q. Wang, and Z. Wang, Sci. China Inf. Sci. **58**, 129301 (2015).
6. Z. Huang and Y. Ji, Chin. Opt. Lett. **11**, 060603 (2013).
7. Y. S. Eroglu, I. Guvenc, N. Pala, and M. Yusksel, in *Proceedings of Wireless and Microwave Technology Conference* (2015), p. 1.
8. T. H. Do, J. Hwang, and M. Yoo, in *Proceedings of International Conference on Ubiquitous and Future Networks* (2013), p. 456.
9. X. Sun, J. Duan, Y. Zou, and A. Shi, Photon. Res. **3**, 296 (2015).
10. M. Yasir, S. Ho, and B. N. Vellambi, J. Lightwave Technol. **32**, 3306 (2014).
11. Z. Huang and Y. Ji, Chin. Opt. Lett. **10**, 050602 (2012).
12. S. Kim and H. Lee, Chin. Opt. Lett. **12**, 120601 (2014).
13. X. Huang, X. Fu, and W. Xu, Electron Lett. **51**, 268 (2015).
14. Y. Liu, C. Hsu, H. Chen, K. Liang, C. Chow, and C. Yeh, Opt. Eng. **54**, 120502 (2015).
15. P. Luo, Z. Ghassemlooy, H. L. Minh, A. Khalighi, X. Zhang, M. Zhang, and C. Yu, in *Proceedings of International Workshop of Optical Wireless Communications* (2014), p. 55.
16. H. Y. Kim, D. H. Kwon, S. H. Yang, Y. H. Son, and S. K. Han, in *Proceedings of International Conference on Optical Internet* (2014), p. 1.
17. X. Zhang, J. Duan, Y. Fu, and A. Shi, J. Lightwave Technol. **32**, 4180 (2014).
18. T. Komine and M. Nakagawa, IEEE Trans. Consum. Electron. **50**, 100 (2004).
19. M. Jiang, Z. Huang, J. Li, R. Zhang, and Y. Ji, Opt Rev. **22**, 294 (2015).